

**Ion-beam channeling yields of host and impurity atoms in LiNbO<sub>3</sub>: Computer simulations**

L. Rebouta\*

*Centro de Física Nuclear da Universidade de Lisboa, Avenida Professor Gama Pinto 2, 1699 Lisboa, Portugal*

P. J. M. Smulders and D. O. Boerma

*Nuclear Solid State Physics, Materials Science Centre, Groningen University, Nijenborgh 4, 9747 AG Groningen, The Netherlands*

F. Agulló-Lopez

*Departamento de Física Aplicada, C-IV, Universidad Autónoma de Madrid, Cantoblanco, 28049 Madrid, Spain*

M. F. da Silva

*Departamento de Física, Instituto de Ciências e Engenharia Nucleares, Laboratório Nacional de Engenharia e Tecnologia Industrial, 2685 Sacavém, Portugal*

J. C. Soares

*Centro de Física Nuclear da Universidade de Lisboa, Av. Prof. Gama Pinto 2, 1699 Lisboa, Portugal*

(Received 20 January 1993)

A Monte Carlo program for the simulation of channeling phenomena in LiNbO<sub>3</sub> crystals is described. Results of the program are compared with experimental yields for Nb, Li, and O from angular scans through the  $\langle 0001 \rangle$ ,  $\langle 02\bar{2}1 \rangle$ ,  $\langle 0\bar{4}41 \rangle$ , and  $\langle 11\bar{2}0 \rangle$  axial directions and through the (0001) planar direction obtained with 1.6-MeV He<sup>+</sup> and proton beams. A set of calculated angular scans for different axial and planar directions, and different impurity locations in LiNbO<sub>3</sub>, is presented. The program has been applied to identify the lattice location of Nd, Eu, and Hf in LiNbO<sub>3</sub>, and that of Lu and Hf in Mg-doped LiNbO<sub>3</sub> by comparing the experimental data with the simulated angular scans. The results confirm that the Hf atoms occupy substitutional Li sites and Eu and Nd atoms lie at a position shifted by  $\approx 0.4$  Å from the regular Li site along the *c* axis and towards the nearest oxygen plane in LiNbO<sub>3</sub>. The Hf and Lu atoms occupy the Nb and Li sites respectively if the LiNbO<sub>3</sub> is codoped with Mg atoms.

**I. INTRODUCTION**

The lattice-site location of impurities in crystals is a subject of considerable interest from a fundamental as well as from a practical viewpoint. In fact, the techniques used in materials engineering to develop new materials for special purposes often rely on the ability to introduce an appropriate impurity into a selected lattice site, either during the crystal growth, or afterwards by ion implantation or diffusion, in order to produce a material with the desired properties.

The channeling technique, combined with Rutherford backscattering (RBS) or nuclear-reaction analysis (NRA), has been a useful tool for studies of the lattice-site location of impurities in metals<sup>1,2</sup> and semiconductors.<sup>3,4</sup> Reliable results may be obtained by a comparison of the experimental data with Monte Carlo simulations.<sup>2,4-6</sup> In favorable cases it is possible to determine the lattice-site position with an accuracy of about 0.02 Å. This accuracy is also achievable for the thermal vibration amplitudes of host and impurity atoms.<sup>7</sup>

In recent years special interest has arisen in the lattice-site location of impurities in oxide compounds such as LiNbO<sub>3</sub>, since the optical properties of these materials are very dependent on the type and the concentration of impurity atoms and, also, on the method of preparation. In fact, it has been shown that the occurrence and the average wave number of the band attri-

buted to OH<sup>-</sup> depend on the lattice site of the impurity atoms.<sup>8</sup> It has also been found that different lattice sites may be occupied by the same kind of impurity atoms, in fractions that are dependent on the codopant introduced during the growth of the crystal.<sup>9</sup>

In order to get precise data, both for the characterization of the crystal lattice of the host atoms, as well as for the distribution of impurity atoms over possible lattice sites, a Monte Carlo program for the simulation of channeling phenomena in LiNbO<sub>3</sub> was developed. This program is a modification and extension of the program FLUX, developed originally for monoatomic cubic crystals<sup>10</sup> and later extended to the case of di-atomic cubic crystals.<sup>11</sup>

In this paper the philosophy of the program is first presented. Finally, the program is then applied to the analysis of experiments on LiNbO<sub>3</sub> doped with a number of transition-metal and rare-earth impurities. Furthermore, a catalogue of channeling profiles for different axial and planar directions is provided. These are essential for a reliable identification of the positions of impurity atoms in LiNbO<sub>3</sub>, by means of channeling experiments.

**II. DETAILS OF THE LiNbO<sub>3</sub> CRYSTAL STRUCTURE**

Lithium niobate grows congruently (Li/Nb=0.945) or stoichiometrically (Li/Nb= 1.0) from the melt using the Czochralski method. At room temperature the ferroelec-

tric phase has very approximately a trigonal Bravais lattice belonging to the space group  $R\bar{3}c$  and point group  $3m$ :  $3m$  is one unique triad and one set of three symmetry related mirror planes parallel to the triad;  $R\bar{3}c$  is triads, screw triads, and  $c$  glide planes.

The structure can be described using a hexagonal cell with parameters  $a = 5.148 \text{ \AA}$  and  $c = 13.863 \text{ \AA}$ .<sup>12</sup> The oxygen sublattice is built on the basis of a hcp cell with six flat oxygen layers in the unit cell and with the oxygen atoms displaced from the true hexagonal positions. In Fig. 1 two different projections of the structure are shown. In the  $\langle 0001 \rangle$  projection it is evident that the oxygen atoms in one plane form irregular triangles slightly rotated from those in adjacent planes, showing that the real symmetry is 3 instead of  $3m$ . Figure 2 shows part of the unit cell. The oxygen atoms form tetrahedrons and octahedrons. The tetrahedral sites are vacant, whereas  $\frac{2}{3}$  of the octahedral sites are occupied by Li and Nb atoms. The distances from the cations to the nearest oxygen atoms are<sup>13</sup> Nb-O, 1.889 and 2.112  $\text{\AA}$ , and Li-O, 2.068 and 2.238  $\text{\AA}$ . Thus the octahedron occupied by Li is

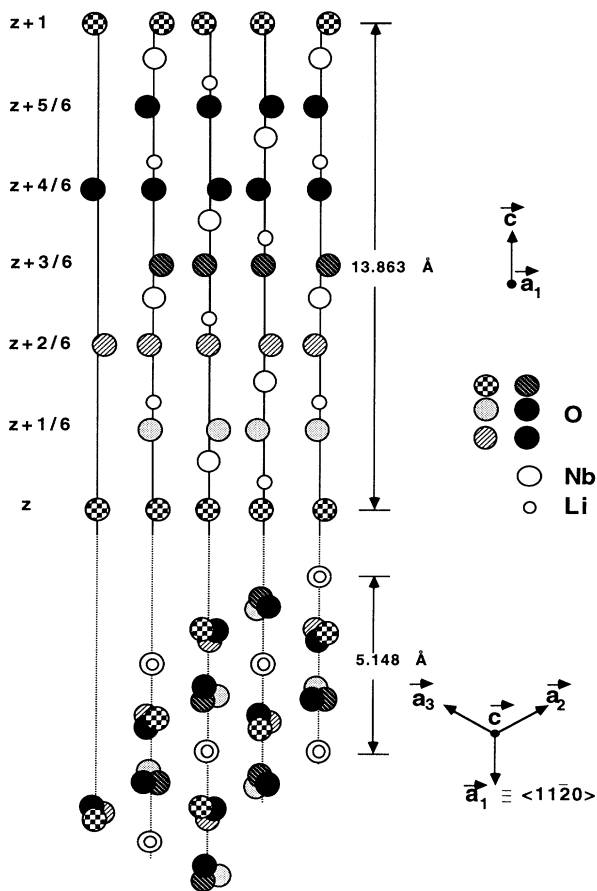


FIG. 1. The hexagonal structure of  $\text{LiNbO}_3$  projected onto the  $\langle 0001 \rangle$  plane (bottom) and onto the  $\langle 11\bar{2}0 \rangle$  plane (top). The atoms of Li and Nb are indicated by small and large open circles. The O positions are shown as circles with various shadings, where each shading pattern corresponds to a certain height along the  $c$  axis.

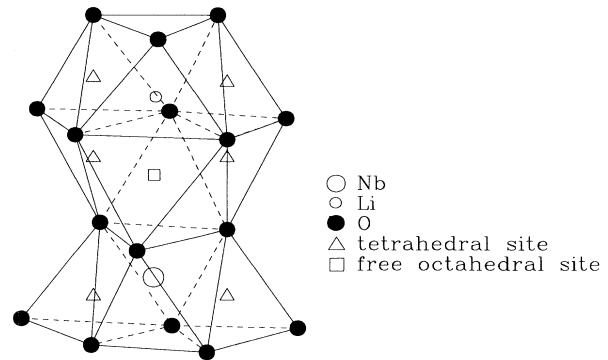


FIG. 2. A part of the unit cell of  $\text{LiNbO}_3$ , illustrating the tetrahedrons and octahedrons formed by the oxygen sublattice. The tetrahedral sites ( $\Delta$ ) are all vacant. The octahedral sites are partly vacant ( $\square$ ) and partly filled by Nb ( $\circ$ ) and Li ( $\circ$ ) atoms.

larger than the Nb octahedron.

The projections of the regular lattice sites on the planes perpendicular to some directions selected for the experiments are shown in Fig. 3. Along the  $\langle 0001 \rangle$  axial direction the Li and the vacant octahedral positions are shadowed by the Nb cations. The oxygen and the tetrahedral lattice sites form a structure with threefold symmetry around the  $c$  axis of the crystal. Along the  $\langle 0441 \rangle$  and  $\langle 01\bar{1}0 \rangle$  directions the projected Li site deviates only slightly from the Nb one. An entirely different situation is observed along the  $\langle 02\bar{2}1 \rangle$  and  $\langle 11\bar{2}0 \rangle$  directions, where Li is near the middle of the channel. The most convenient geometry for the identification of the Li site is the  $\langle 0001 \rangle$  planar direction. In this case the Li sites are just in the middle between the planes formed by Nb and O atoms. In the projections of Fig. 3 the  $\langle 0001 \rangle$  plane corresponds to the horizontal row in the  $\langle 11\bar{2}0 \rangle$  and  $\langle 01\bar{1}0 \rangle$  axial projections as indicated. The  $\langle 11\bar{1}02 \rangle$  plane is in a diagonal direction in the  $\langle 02\bar{2}1 \rangle$  axial projection; see Fig. 3.

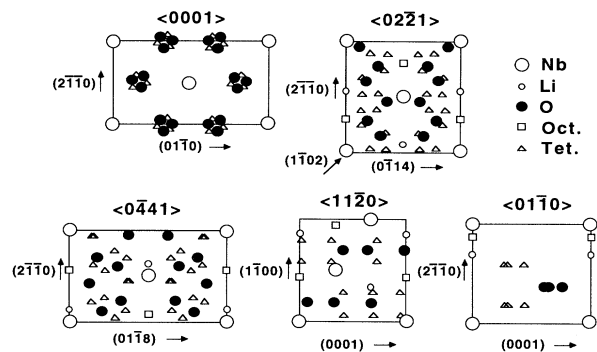


FIG. 3. Projection of regular lattice sites of  $\text{LiNbO}_3$  onto planes perpendicular to directions used in axial channeling experiments. Indicated are the projected sites of Li ( $\circ$ ), Nb ( $\circ$ ), O ( $\bullet$ ), as well as the tetrahedral ( $\Delta$ ) and vacant octahedral ( $\square$ ) sites. Some planar directions are indicated.

### III. SHORT DESCRIPTION OF THE SIMULATION PROGRAM

The basic philosophy of the Monte Carlo simulation program has been described in a previous paper.<sup>10</sup> The program was modified to enable the use of three species of lattice atoms as present in the  $\text{LiNbO}_3$  lattice. The trigonal structure, with its low degree of symmetry made further changes necessary.

The program calculates the trajectories of a large number of individual ions, entering the crystal lattice at random positions with an initial direction close to an axial channeling direction. The ions are assumed to travel along straight lines between collisions. In the original program the distance between the collisions—or rather the distance between planes, perpendicular to the channel, where the ion direction is updated—was constant. This is not the case for the  $\text{LiNbO}_3$  structure and the sequence of distances is now given as input. At these planes the velocity and the position of the ion are updated, taking into account (a) a binary collision with the nearest lattice atom treated in the impulse approximation, (b) the deflection due to surrounding strings situated at larger distances calculated in the thermally modified continuum string approximation,<sup>14</sup> (c) the energy loss due to the interaction with electrons calculated in an impact parameter dependent way,<sup>15</sup> (d) the angular straggling

due to the electronic energy loss, taken into account by a random deflection, and (e) the thermal vibration of each lattice atom is accounted for by a small random displacement from its equilibrium site sampled from an isotropic Gaussian distribution.

In the simulations the Ziegler-Biersack-Littmark (ZBL) universal potential<sup>16</sup> was used. The flux distribution in the plane perpendicular to the channel is accumulated during the simulation and is convoluted with the depth distribution of the impurity atoms for later use in the calculation of the impurity yields. The nuclear encounter probabilities<sup>6</sup> for each of the host lattice atoms, as a function of depth, are also accumulated. Optionally, these may be weighted with an energy-dependent reaction cross section.

For an angular scan the simulation is repeated for each of the points of the scan. The yield for the host lattice atoms may be obtained directly from the nuclear encounter probability averaged over the proper depth interval. As an alternative, the nuclear encounter probability and the calculated energy loss and the straggling, both as a function of depth may be used for a simulation of the energy spectrum. For the impurity atoms the simulated yield for each of the points of the angular scan is obtained from the weighted flux distribution accumulated during the simulation. This flux is convoluted with the assumed distribution of impurity sites, taking into ac-

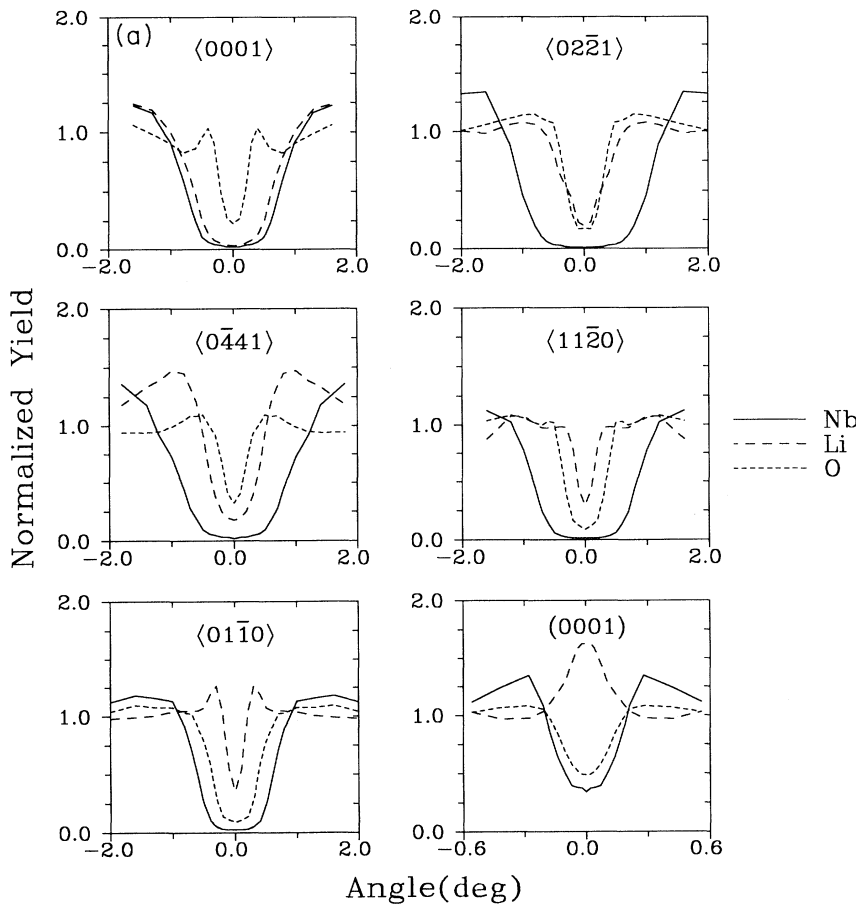


FIG. 4. A catalogue of angular scans for impurities in  $\text{LiNbO}_3$ . Each figure shows  $\langle 0001 \rangle$ ,  $\langle 02\bar{2}1 \rangle$ ,  $\langle 0\bar{4}41 \rangle$ ,  $\langle 11\bar{2}0 \rangle$ , and  $\langle 01\bar{1}0 \rangle$  axial scans and a  $\langle 0001 \rangle$  planar scan, for 1.6-MeV  $\text{He}^+$  ions, averaged over a depth of 1000 Å, in scan planes specified in the text. (a) Host lattice atoms Li, Nb, and O. (b) Heavy impurity at Li site, octahedral site, and tetrahedral site. Scans for host Nb atoms are shown for comparison. (c) Heavy impurity shifted from the Li site in the  $\langle 0001 \rangle$  direction by 0 to  $+0.5$  Å. Scans for host Nb atoms are shown for comparison. The plus sign indicates a shift in the direction away from the nearest oxygen plane. (d) Heavy impurity, shifted from the Li site in the  $\langle 0001 \rangle$  direction by 0 to  $-0.5$  Å. The minus sign indicates a shift in the direction to the nearest oxygen plane. (e) As Fig. 5(d), for shifts of  $-0.7$  to  $-1.3$  Å.

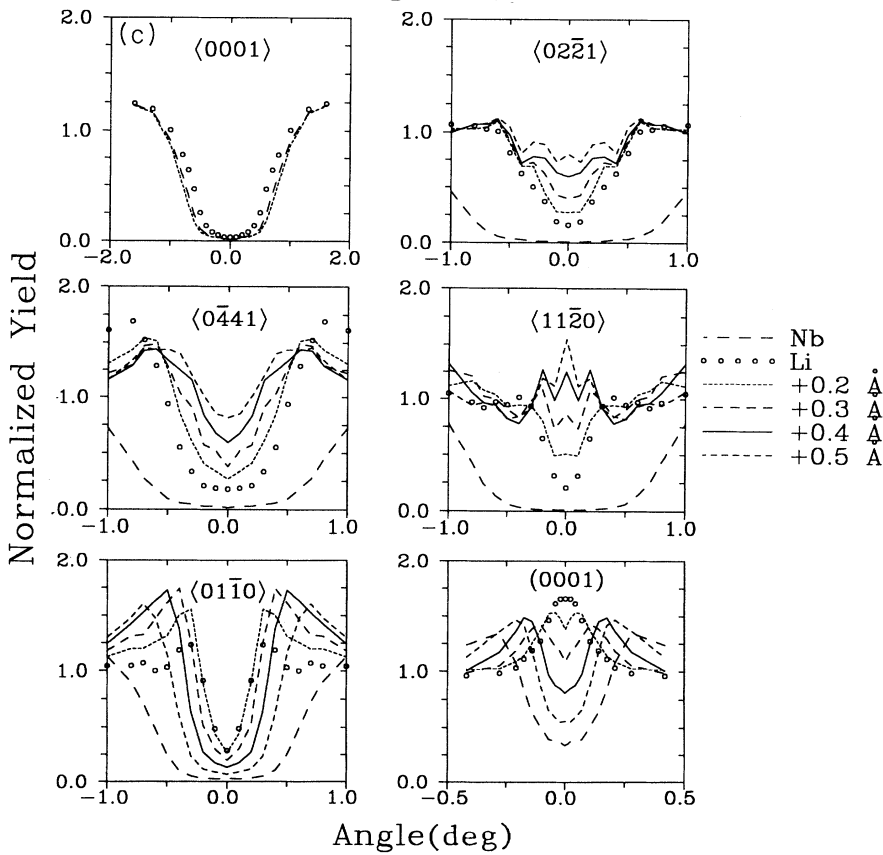
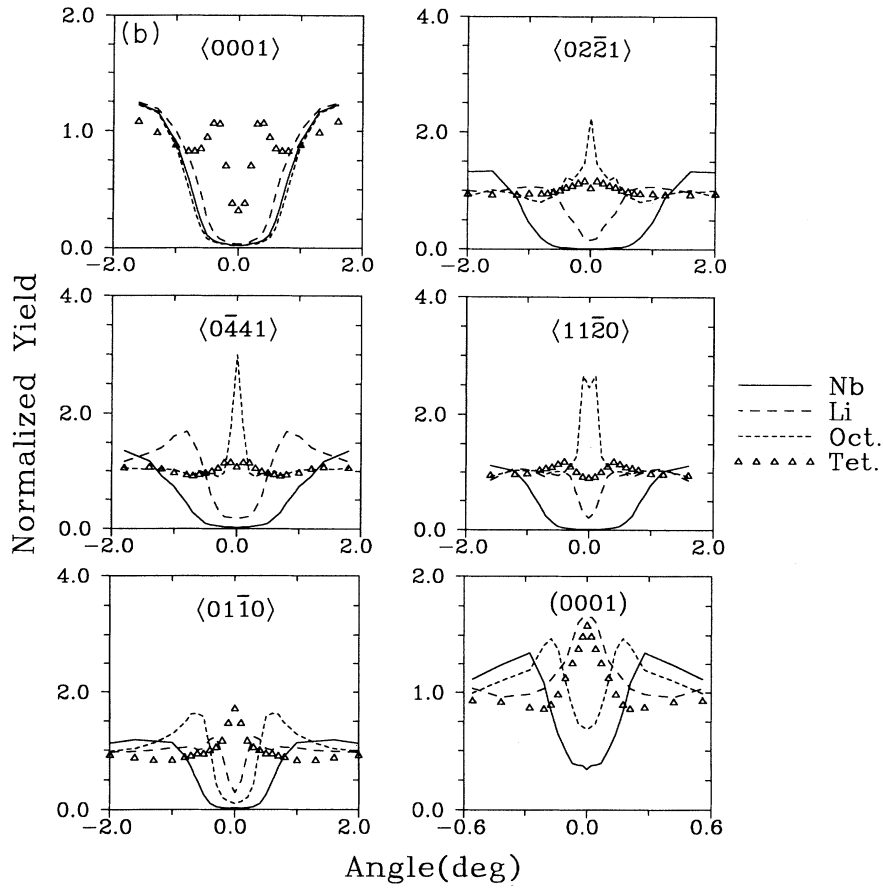


FIG. 4. (Continued).

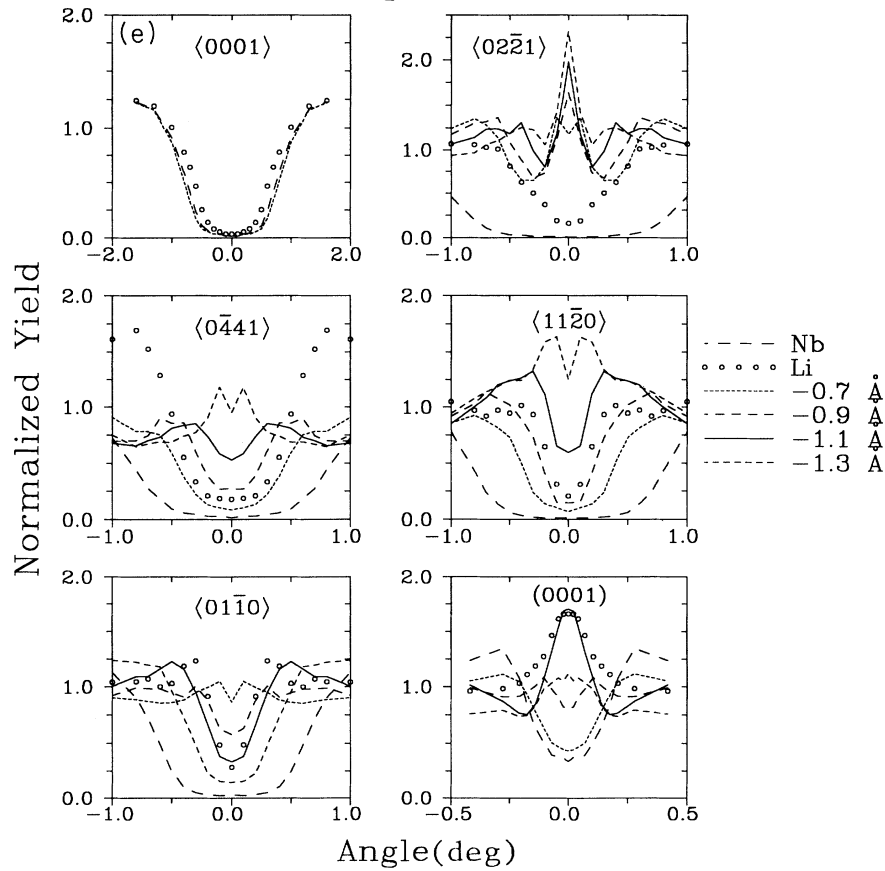
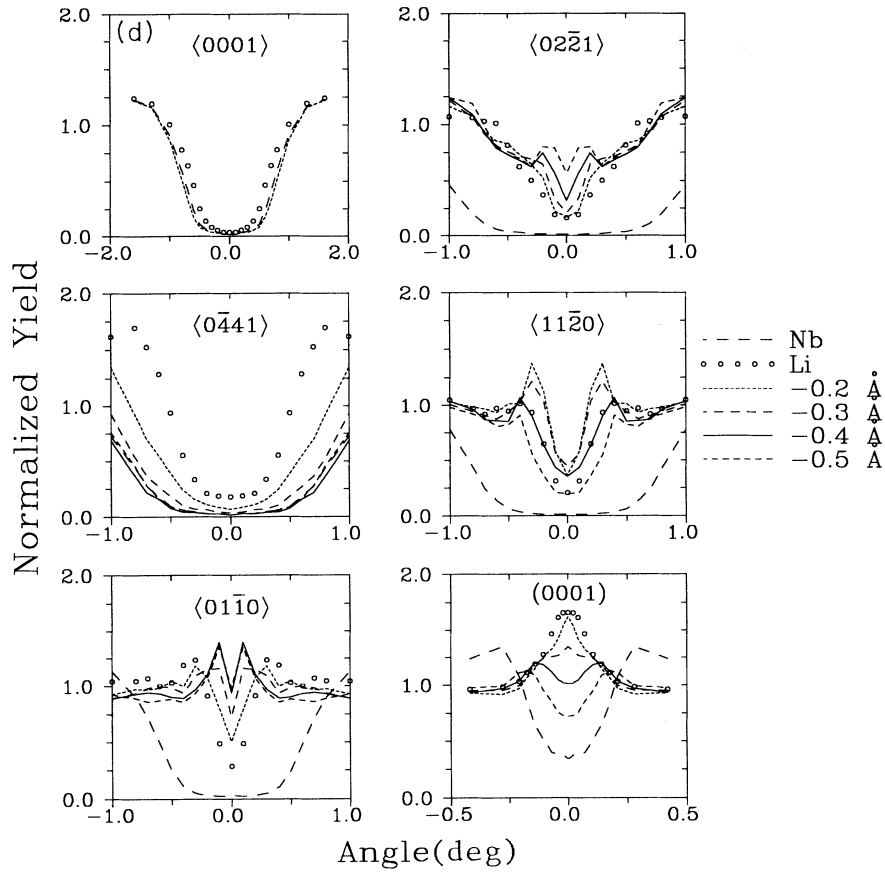


FIG. 4. (Continued).

count the thermal vibrations and averaging over equivalent projected sites. Thus, it is possible to vary the assumed positions of the impurity atoms, as well as their vibration amplitude without having to repeat the time consuming simulation of the flux distribution. For details see Ref. 10.

#### IV. A CATALOGUE OF SIMULATED ANGULAR SCANS IN $\text{LiNbO}_3$

In this section we present a catalogue of angular scans around various axial and planar directions, using 1.6-MeV He ions. The simulations include substitutional host positions, Fig. 4(a), as well as the vacant octahedral and tetrahedral locations, Fig. 4(b). Moreover, we have also simulated angular scans for impurity atoms displaced from the regular Li site in either sense along the  $c$  axis, Figs. 4(c), 4(d), and 4(e). The reason to present these off-substitutional scans is that some previous experimental data suggest that impurities occupying the Li octahedron may be displaced from the exact substitutional site. This behavior is possibly associated to the much shallower potential at the Li site in comparison to that of the Nb site.

Angular scans were simulated through the  $\langle 0001 \rangle$ ,  $\langle 02\bar{2}1 \rangle$ ,  $\langle 04\bar{4}1 \rangle$ ,  $\langle 11\bar{2}0 \rangle$ , and  $\langle 01\bar{1}0 \rangle$  axes and across the (0001) plane. The following planes were used for the axial scans: for the  $\langle 0001 \rangle$  axis a plane  $50^\circ$  away from the  $(01\bar{1}0)$  plane, for the  $\langle 02\bar{2}1 \rangle$  axis  $60^\circ$  away from the  $(0\bar{1}14)$  plane, for the  $\langle 04\bar{4}1 \rangle$  axis  $20^\circ$  away from the  $(01\bar{1}8)$  plane, for the  $\langle 11\bar{2}0 \rangle$  axis  $12^\circ$  away from the (0001) plane, and for the  $\langle 01\bar{1}0 \rangle$  axis  $15^\circ$  away from the (0001) plane. The planar scan through the (0001) plane was calculated with an incident direction making an angle of  $4^\circ$  with the  $\langle 11\bar{2}0 \rangle$  axis.

For each point 5000 trajectories were simulated over a depth of 1000 Å. The rms vibration amplitudes used in the simulations of Fig. 4 are  $u_2 = 0.09(1)$  Å,  $0.15(2)$  Å,

and  $0.12(2)$  Å for Nb, Li, and O, respectively. They yield the best agreement with the angular scans for host ions in Fig. 5. However, for Figs. 4(b), 4(c), 4(d), and 4(e) a value  $u_2 = 0.07$  Å for the vibrational amplitude of the impurity was used. The choice of this value is related with the simulations for Hf atoms discussed in Sec. VI. For comparison the scans for Nb are also shown.

It is evident that the patterns for different sites are quite different. Therefore, a set of channeling measurements in the geometries as described above should be sufficient to distinguish between possible lattice sites in most cases.

#### V. COMPARISON WITH EXPERIMENTAL ANGULAR SCANS IN $\text{LiNbO}_3$

As a test case for the simulations of the host lattice atoms in  $\text{LiNbO}_3$  we chose a previously reported experiment,<sup>17</sup> although the  $\text{LiNbO}_3$  sample used in that work was doped with 6 mol % of Mg and 0.8 mol % of Er. The Nb and O yields were measured by detecting elastically scattered protons (RBS). The Li yield was determined using the  ${}^7\text{Li}(p,\alpha){}^4\text{He}$  nuclear reaction. The energy of the proton beam was 1.6 MeV.

Angular scans were measured through the  $\langle 0001 \rangle$ ,  $\langle 02\bar{2}1 \rangle$ ,  $\langle 04\bar{4}1 \rangle$ , and  $\langle 11\bar{2}0 \rangle$  axes, and across the (0001) planar direction. The scan angle for the  $\langle 0001 \rangle$  axis was  $52^\circ$  from the  $(01\bar{1}0)$  plane, and for the  $\langle 04\bar{4}1 \rangle$  axis it was  $12^\circ$  from the  $(01\bar{1}8)$  plane. The angular scans through the  $\langle 02\bar{2}1 \rangle$  and  $\langle 11\bar{2}0 \rangle$  axes were taken in the  $(1\bar{1}02)$  and (0001) planes, respectively. The planar scan through the (0001) plane was taken at  $4^\circ$  from the  $\langle 11\bar{2}0 \rangle$  axis.

For the beam divergence a standard deviation of  $0.03^\circ$  was assumed. This includes the beam spread due to a disordered surface layer. The thermal vibration amplitudes were as for Fig. 4(a). For the calculation of the flux a square grid with a grid size of  $0.04$  Å was used. The two-dimensional cells used in the calculations are shown

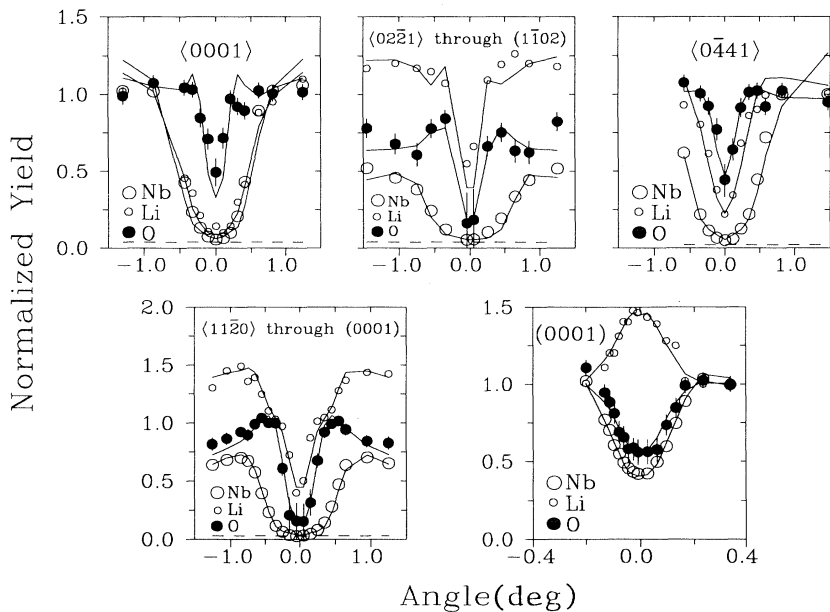


FIG. 5. Channeling experiments on the host atoms of  $\text{LiNbO}_3$  compared with simulations. Angular scans are given for Li, Nb, and O atoms, through the  $\langle 0001 \rangle$ ,  $\langle 02\bar{2}1 \rangle$ ,  $\langle 04\bar{4}1 \rangle$ , and  $\langle 11\bar{2}0 \rangle$  axes and also across the (0001) plane. For further details, see text.

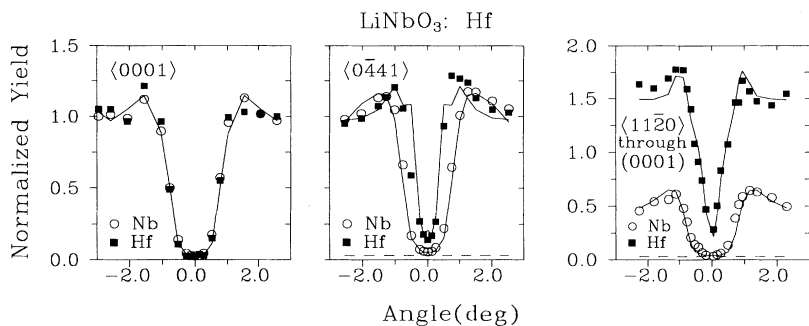


FIG. 6. Experimental and simulated angular scans for the Nb host atoms ( $\circ$ ) and Hf impurity atoms ( $\square$ ), of channeling of 1.6-MeV  $\text{He}^+$  ions in  $\text{LiNbO}_3$  doped with 1.3% Hf through three major axes as indicated. The solid lines for Hf are simulations for the Li site.

in Fig. 3. The large number of atoms, for which binary collisions are evaluated, results in a considerable computation time. For example, for the case of the  $\langle 0001 \rangle$  axis, 18 binary collisions are considered over a distance of  $d = 13.863 \text{ \AA}$ . For each calculated point 2000 trajectories were followed until a depth of 4500  $\text{\AA}$ . The time for the calculation of a complete angular scan was 24 h using an Olivetti M300-30 PC, i-486 running at 25 MHz. The experimental points were obtained from a window in the spectra corresponding to the same thickness.

The comparison of the simulations described in Sec. IV with the experimental data is presented in Fig. 5. The experimental yields are represented by symbols and the calculated scans by the solid lines. For Nb and Li the simulated scans show a good agreement for the width and slope of the channeling dips. The simulated minimum yield for Nb is somewhat lower than observed experimentally. This effect may be due to a small amount of structural defects in the  $\text{LiNbO}_3$  lattice. Therefore, a small random fraction of 2–3% was added to the simulations, as indicated by dashed lines. The agreement for some of the oxygen dips is worse. The evaluation of the yield for oxygen from the RBS spectra requires assumptions about the shape of the underlying background of protons scattered from Nb. This leads to relatively large errors and might also be the cause for the small systematic deviations seen in Fig. 5.

In general, the agreement is satisfactory. In particular, the flux peak of the Li signal in the  $\langle 0001 \rangle$  plane, and also the enhanced yield for Li in the shoulders of the  $\langle 11\bar{2}0 \rangle$  scan in the  $\langle 0001 \rangle$  plane, are well reproduced.

## VI. LATTICE SITE LOCATION OF Hf IN CONGRUENT $\text{LiNbO}_3$ AND OF Lu AND Hf IN Mg CODOPED $\text{LiNbO}_3$

The samples used in the experiments had been doped during growth with 1.3 mol % Hf. Angular scans for Nb and Hf were measured with a 1.6-MeV  $\text{He}^+$  beam, through the  $\langle 0001 \rangle$ ,  $\langle 0\bar{4}41 \rangle$ , and  $\langle 11\bar{2}0 \rangle$  axes. The scan plane for the  $\langle 0001 \rangle$  axis made an angle of  $50^\circ$  with a  $\langle 01\bar{1}0 \rangle$  plane. For the  $\langle 0\bar{4}41 \rangle$  axis the scan plane was  $20^\circ$  from a  $\langle 01\bar{1}8 \rangle$  plane. The scan through the  $\langle 11\bar{2}0 \rangle$  axis was taken in the  $\langle 0001 \rangle$  plane. The experimental results were normalized to random spectra obtained, while rotating the sample around the axial channeling direction at an angle of  $4^\circ$  with the beam direction.

The same angular scans were simulated. The thermal vibration amplitudes  $u_2$  assumed for Li, Nb, and O, were 0.15, 0.09, and 0.12  $\text{\AA}$ , respectively, as discussed in the previous sections. The Nb and Li atoms are surrounded by six oxygen atoms, and considering that the heavier Hf atoms have a similar surrounding, we assumed a thermal vibration amplitude for Hf ions of 0.07  $\text{\AA}$ , somewhat smaller than the value used for Nb atoms. For each calculated point 5000 trajectories were simulated over a depth of 1000  $\text{\AA}$ . The calculated and experimental yields obtained are presented in Fig. 6. The experimental yields are shown by symbols as indicated and the calculated yields are given by solid lines. The simulated Nb yields show a good agreement with the experiments. However, a random fraction of 2–3% is, again, needed to fit the minimum yields. The deviations observed in the scan

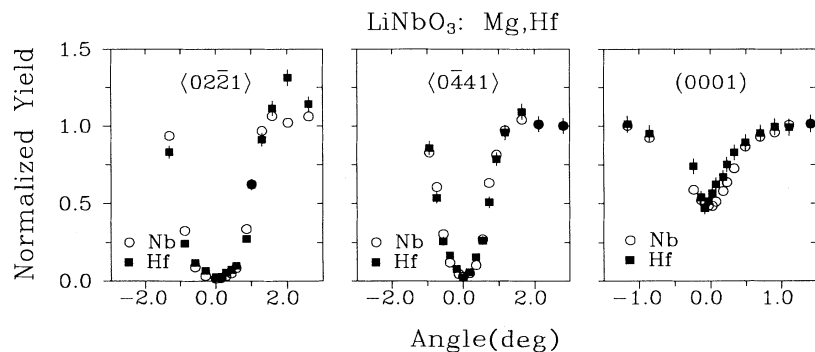


FIG. 7. Experimental angular scans for the Nb host atoms ( $\circ$ ) and Hf impurity atoms ( $\square$ ), of channeling of 1.6-MeV  $\text{He}^+$  ions in  $\text{LiNbO}_3$  doped with 1% Hf and codoped with 6% Mg, through the major axes and one plane, as indicated. It is evident that the Hf atoms occupy the Nb site.

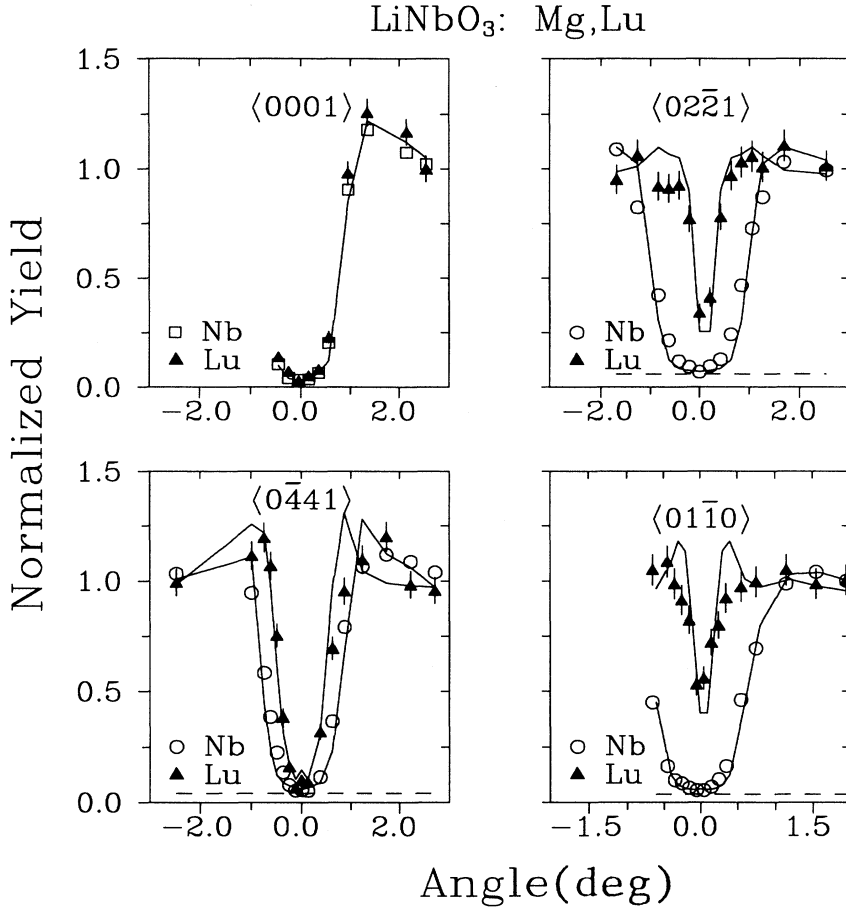


FIG. 8. Experimental and simulated angular scans for Nb ( $\circ$ ) and Lu ( $\triangle$ ) taken through four axial directions as indicated, for a LiNbO<sub>3</sub> sample codoped with 0.76% Lu and 5.2% Mg. The solid lines for Lu are simulated angular scans for the Li site.

through the  $\langle 11\bar{2}0 \rangle$  axis are probably due to the radiation damage caused by the analyzing beam. These simulations had to be multiplied by a factor between 0.8 and 1.0 to fit the experimental results. The cause of this discrepancy is not known.

The comparison between the experimental Hf and Li yields obtained for angular scans across  $\langle 0\bar{4}41 \rangle$  and  $\langle 11\bar{2}0 \rangle$  axes suggests that Hf atoms occupy Li sites. Moreover, the simulated Hf yields for this assumption show an excellent agreement with the experimental data. This confirms that the Hf atoms in LiNbO<sub>3</sub> occupy Li positions, as was already concluded in Ref. 18. On the other hand, the nice agreement indicates that the assumed value of  $u_2 = 0.07$  Å for the thermal vibration amplitude of the Hf atoms is reasonable. In the following this value will be adopted for all heavy impurities.

It is remarkable that the Hf atoms in the Mg-codoped LiNbO<sub>3</sub> do not occupy the Li site, as may be inferred from the angular scan through the (0001) plane shown in Fig. 7. In this scan and also in those through the  $\langle 02\bar{2}1 \rangle$  and  $\langle 0\bar{4}41 \rangle$  axes, presented in the same figure, the normalized yields of Hf and Nb as a function of angle are very similar. Consequently, it is safely concluded that Hf atoms occupy the Nb site in Mg-codoped LiNbO<sub>3</sub>.

In Fig. 8 the  $\langle 0001 \rangle$ ,  $\langle 02\bar{2}1 \rangle$ ,  $\langle 0\bar{4}41 \rangle$ , and  $\langle 01\bar{1}0 \rangle$  scans from Nb and Lu are shown for the LiNbO<sub>3</sub> sample codoped with Mg. A qualitative comparison of the mea-

sured angular scans for the Lu atoms with those calculated for the Li site suggests that Lu occupies the Li substitutional position. This is, indeed, confirmed by the results of the simulation. The solid lines shown in Fig. 8 represent the close encounter probability for Lu atoms at the Li site. The simulated and experimental widths of the dips agree quite well, although the shoulders show small deviations possibly due to a small difference in the scan angle. The general agreement between experimental and calculated yields is good. Therefore, we conclude that Lu atoms are predominantly at the Li sites.

## VII. LATTICE SITE LOCATION OF Eu AND Nd IN CONGRUENT LiNbO<sub>3</sub>

Angular scans for Nd and Eu taken through the  $\langle 0001 \rangle$ ,  $\langle 02\bar{2}1 \rangle$ ,  $\langle 0\bar{4}41 \rangle$ , and  $\langle 01\bar{1}0 \rangle$  axial directions and (0001) planar direction are presented in Fig. 9. The results from the  $\langle 0001 \rangle$  angular scan show that Eu ions lie along the rows defined by Nb ions. From the  $\langle 0\bar{4}41 \rangle$  angular scan results we exclude the occupation of a position in the neighborhood of the free octahedral site [see Fig. 4(b)]. In the angular scan through the  $\langle 01\bar{1}0 \rangle$  axis the Eu angular profile has a minimum value of about 1. As we can see from the simulations presented in Fig. 4(a) this result is not compatible with a location of the Eu atoms at the Nb or at the Li site. It is also inconsistent

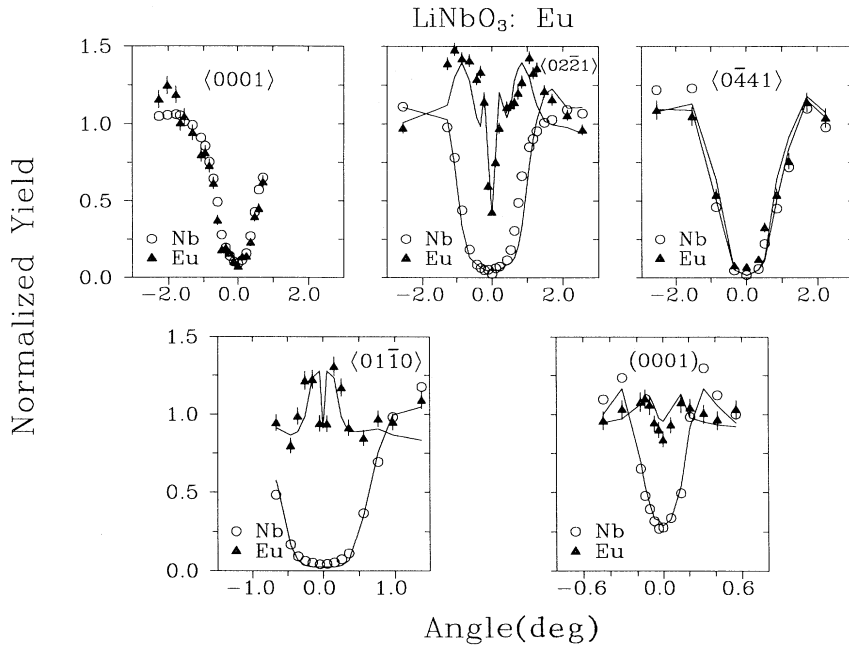


FIG. 9. Experimental and simulated angular scans for Nb ( $\circ$ ) and Eu ( $\triangle$ ), taken through four axial directions and one planar direction as indicated, for a congruent LiNbO<sub>3</sub> sample doped with 0.8% Eu. The solid lines for Eu are simulations for the assumption that the Eu atoms occupy positions shifted by 0.4 Å from the Li site towards the nearest oxygen plane.

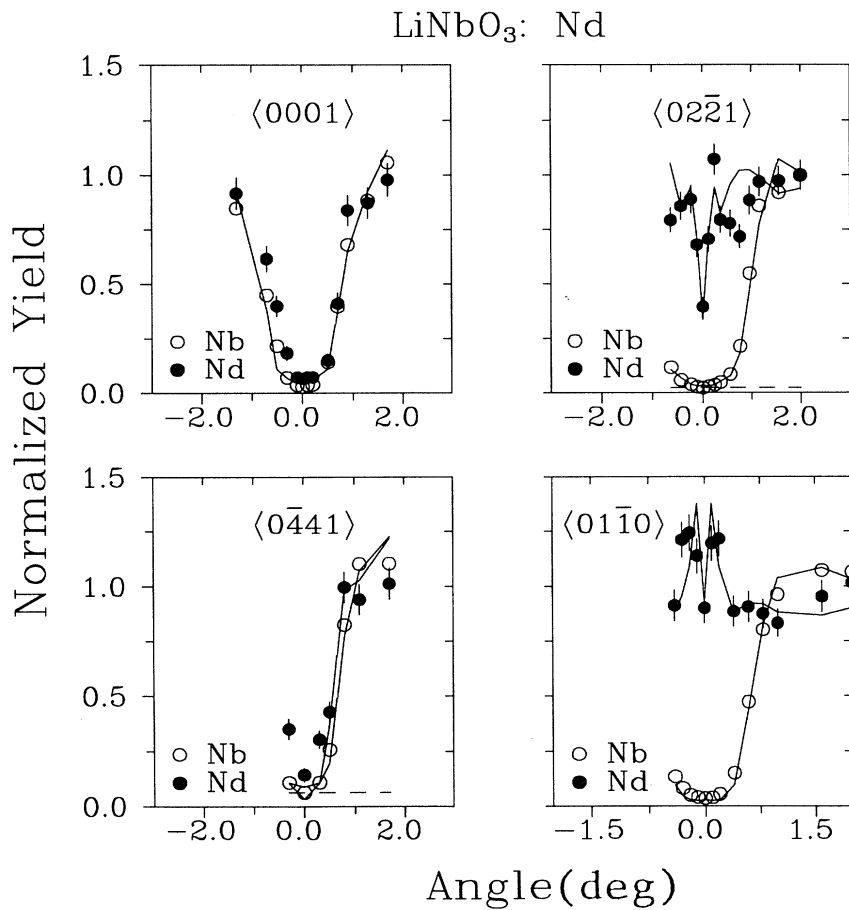


FIG. 10. Experimental and simulated angular scans for Nb ( $\circ$ ) and Nd ( $\bullet$ ) taken through four axial directions as indicated for a congruent LiNbO<sub>3</sub> sample doped with 0.4% Nd. The solid lines for Nd are simulations for the assumption that the Nd occupy positions shifted by 0.4 Å from the Li site towards the nearest oxygen plane.

with a mixture of two fractions of Eu atoms at both positions as it was previously proposed.<sup>18</sup>

The simulations represented in Fig. 4(d) suggest that Eu ions occupy a position shifted from the regular Li position towards the nearest oxygen plane with a shift between 0.3 and 0.5 Å. For a more quantitative assessment, we compared the experimental data and the calculated yields corresponding to a position shifted by 0.4 Å from the Li site. The good fit obtained, as shown by the solid lines in Fig. 9, unambiguously confirms the deviated position of Eu with regard to the host location.

Figure 10 shows the angular scans through the  $\langle 0001 \rangle$ ,  $\langle 02\bar{2}1 \rangle$ ,  $\langle 0441 \rangle$ , and  $\langle 01\bar{1}0 \rangle$  axes measured for Nd-doped LiNbO<sub>3</sub>. Like in the Eu case the similarity of Nd and Nb angular profiles in the scans of  $\langle 0001 \rangle$  and  $\langle 0441 \rangle$  axes shows that Nd atoms do not occupy the free octahedral site and should be in the Nb rows along the *c* axis. On the other hand the Nd angular profiles obtained in the scans through the  $\langle 01\bar{1}0 \rangle$  and  $\langle 02\bar{2}1 \rangle$  axes are similar to the Eu profiles obtained through the same directions. Thus, we can conclude that Nd and Eu atoms occupy the same site, i.e., a position shifted  $\approx 0.4$  Å from the Li site towards the nearest oxygen plane.

### VIII. DISCUSSION AND CONCLUSIONS

A computer program has been developed and tested to simulate channeling experiments in LiNbO<sub>3</sub>. Both the angular scans for the host atoms as well as the impurities located at various sites are well reproduced with the program. The catalogue of angular scans for different impurity sites presented here constitutes a useful guide to identify the lattice position from channeling data and can help to plan experiments to distinguish between different possible lattice sites. As a summary of the investigation, the lattice sites occupied by impurity atoms in LiNbO<sub>3</sub> and LiNbO<sub>3</sub> doped with Mg are presented in Table I. It appears that there is a strong tendency for the cation impurities to occupy Li lattice sites, either substitutionally or shifted. This behavior is independent of the valence

state of the impurity, ruling out any change misfit arguments to determine location. In principle, one might relate that preference to the phase diagram of LiNbO<sub>3</sub>. In fact, homogeneous crystals grow at the congruent composition, presenting a few percent Li deficiency. Therefore, impurities will preferentially find empty Li sites during the incorporation process. This argument could be tested by investigating site locations in stoichiometric crystals and this study is now underway in our laboratory. Anyhow considering that impurity atoms in the LiNbO<sub>3</sub> structure are surrounded by oxygen atoms, we have looked for a correlation between the lattice site of the impurity and its cation-oxygen bond length in the oxide, as presented in Table II. These bond lengths have been compared with the mean value  $R_{\text{Li-O}}$  of the two Li-O distances in congruent LiNbO<sub>3</sub> (see Sec. II), and with the mean value  $R_{\text{Nb-O}}$ , defined similarly. These values are also given in Table II. It seems that all impurities with an oxygen-bond length exceeding  $R_{\text{Nb-O}}$  occupy Li sites, or shifted Li sites if the bond length also exceeds  $R_{\text{Li-O}}$ . Impurities with a bond length smaller than or equal to  $R_{\text{Nb-O}}$  can occupy either Li or Nb sites. The observation that Hf occupies Li sites in undoped LiNbO<sub>3</sub> and Nb sites in Mg-doped LiNbO<sub>3</sub> may be explained by the large number of empty Li sites in undoped congruent crystals. In fact, it has been shown that the Li deficiency ( $\approx 6\%$ ) in these crystals is compensated with the presence of Nb at the Li site, forming Nb<sub>Li</sub> antisites.<sup>13</sup> The incorporation of the cation impurities should imply the occupation of Li empty places, preventing the formation of those Nb<sub>Li</sub> antisites. With the Mg-doping and under the assumption that all Nb<sub>Li</sub> antisites are replaced by Mg atoms, the occupation of the Nb site by Hf ions becomes energetically favorable. In order to check this model, similar experiments comparing the behavior of other impurities in LiNbO<sub>3</sub> and Mg-doped LiNbO<sub>3</sub> should be carried out.

The analysis of the data shows that the channeling technique is quite sensitive to the value of the thermal vibration amplitudes of the host atoms. In fact, a precision

TABLE I. Summary of lattice sites for impurities in LiNbO<sub>3</sub> and LiNbO<sub>3</sub>: Mg. In the last column a reference to the present work is indicated by a *p*.

Impurity	Lattice site		Ref.
	LiNbO <sub>3</sub>	LiNbO <sub>3</sub> :Mg	
Ta	Nb		18,19
Fe	Li		20
Ti	Li		21,22,23
Mn	Li		24
Ni	Li		22
Hf	Li	Nb	18,19, <i>p</i>
In		Li	25
Lu		Li	25, <i>p</i>
Tm		Li + random ( $\approx 10\%$ )	26
Er	Shifted from Li??	Li	17
Gd		Li octahedron + random ( $\approx 70\%$ )	26
Eu	Shifted from Li ( $\sim 0.4$ Å)	Shifted from Li	<i>p</i>
Nd	Shifted from Li ( $\sim 0.4$ Å)		<i>p</i>

TABLE II. Values of cation-oxygen distances in the oxides of impurity elements (Ref. 27). The meaning of  $R_{\text{Li-O}}$  and  $R_{\text{Nb-O}}$  is given in the text.

Oxide	$d$ (Å)	Oxide	$d$ (Å)
Li <sub>2</sub> O	2.004	Fe <sub>2</sub> O <sub>3</sub>	2.02
Nb <sub>2</sub> O <sub>5</sub>	1.888	In <sub>2</sub> O <sub>3</sub>	2.17
Ta <sub>2</sub> O <sub>5</sub>	1.83	Lu <sub>2</sub> O <sub>3</sub>	2.23
MgO	2.106	Tm <sub>2</sub> O <sub>3</sub>	2.25
MnO <sub>2</sub>	1.877	Er <sub>2</sub> O <sub>3</sub>	2.26
NiO	2.084	Gd <sub>2</sub> O <sub>3</sub>	2.32
TiO <sub>2</sub>	1.966	Eu <sub>2</sub> O <sub>3</sub>	2.33
HfO <sub>2</sub>	2.021	Nd <sub>2</sub> O <sub>3</sub>	2.38
$R_{\text{Li-O}}$	2.15	$R_{\text{Nb-O}}$	2.00

of 11% of Nb, 13% for O, and 17% for Li has been obtained in the simulations of the results presented in Fig. 4. This high sensitivity gives a unique possibility for a systematic study of the vibration amplitudes associated with particular sites of the LiNbO<sub>3</sub> lattice. However, it should be kept in mind that experimental values for the vibration amplitude may contain a component due to small static displacements.

The values of the thermal vibration amplitudes found

in the present work are very close to those determined by x-ray diffraction in stoichiometric LiNbO<sub>3</sub>.<sup>13</sup> This suggests that in our doped congruent crystals the lattice potential at ion sites is about the same as in stoichiometric crystals.

In Ref. 13 it is shown that the thermal vibration amplitudes are anisotropic, with a maximum anisotropy in the purely congruent phase. This conclusion is not supported by our data. In fact, good agreement between simulation and experiment has been obtained with one and the same set of isotropic vibration amplitudes for all angular scans. In the same reference the Li thermal vibration amplitude was found to be higher in congruent than in stoichiometric LiNbO<sub>3</sub> crystals. This may be due to small static displacements of the Li atoms in this latter case. The channeling technique will be used to test this effect in the near future.

#### ACKNOWLEDGMENTS

This work has been carried out with partial support from the bilateral cultural agreement between Portugal and The Netherlands and with a NATO grant for collaborative research (CRG.890934) with the Autonoma University of Madrid, Spain. One of us (L.R.) thanks the Junta Nacional de Investigação Científica e Tecnológica (JNICT) for a grant, under the CIENCIA Program.

\*Present address: Dep. de Física, Universidade do Minho, Azurém, 4800 Guimarães, Portugal.

<sup>1</sup>R. Vianden, E. N. Kaufmann, and J. W. Rodgers, *Phys. Rev. B* **22**, 63 (1980).

<sup>2</sup>W. Segeth, D. O. Boerma, L. Niesen, and P. J. M. Smulders, *Phys. Rev. B* **39**, 10 725 (1989).

<sup>3</sup>B. Bech Nielsen, *Phys. Rev. B* **37**, 6353 (1988).

<sup>4</sup>P. J. Smulders, D. O. Boerma, B. Bech Nielsen, and M. L. Swanson, *Nucl. Instrum. Methods B* **45**, 438 (1990).

<sup>5</sup>R. Vianden, P. M. J. Winand, E. N. Kaufmann, J. R. Macdonald, and T. E. Jackmann, *Nucl. Instrum. Methods B* **7/8**, 109 (1985).

<sup>6</sup>J. H. Barret, *Phys. Rev. B* **3**, 1527 (1971).

<sup>7</sup>A. Dygo and A. Turos, *Phys. Rev. B* **40**, 7704 (1989).

<sup>8</sup>L. Kovacs, Zs. Szaller, I. Cravero, I. Foldvari, and C. Zaldo, *J. Phys. Chem. Solids* **51**, 417 (1990).

<sup>9</sup>L. Rebouta, M. F. da Silva, J. C. Soares, J. A. Sanz-García, E. Diéguez, and F. Agulló-Lopez, *Nucl. Instrum. Methods B* **64**, 189 (1992).

<sup>10</sup>P. J. M. Smulders and D. O. Boerma, *Nucl. Instrum. Methods B* **29**, 471 (1987).

<sup>11</sup>P. J. Smulders, D. O. Boerma, and M. Shaanan, *Nucl. Instrum. Methods B* **45**, 450 (1990).

<sup>12</sup>H. Megaw, *Acta Crystallogr. A* **24**, 583 (1968).

<sup>13</sup>S. C. Abrahams and P. Marsh, *Acta Crystallogr. B* **42**, 6 (1986).

<sup>14</sup>B. R. Appleton, C. Erginsoy, and W. M. Gibson, *Phys. Rev.* **161**, 330 (1967).

<sup>15</sup>K. Detmann and M. T. Robinson, *Phys. Rev. B* **10**, 1 (1974).

<sup>16</sup>J. P. Biersack and J. F. Ziegler, *Nucl. Instrum. Methods* **194**, 93 (1982).

<sup>17</sup>L. Kovacs, L. Rebouta, J. C. Soares, and M. F. da Silva, *Rad. Effects Def. Sol.* **119-121**, 445 (1991).

<sup>18</sup>L. Rebouta, M. F. da Silva, J. C. Soares, J. A. Sanz-García, E. Diéguez, and F. Agulló-Lopez, *J. Mater. Res.* **7**, 1 (1992).

<sup>19</sup>C. Prieto, C. Zaldo, P. Fessler, H. Dexpert, J. A. Sanz-García, and E. Diéguez, *Phys. Rev. B* **43**, 2594 (1991).

<sup>20</sup>L. Rebouta, M. F. da Silva, J. C. Soares, M. Hage-Ali, J. P. Stoquert, P. Siffert, J. A. Sanz-García, E. Diéguez, and F. Agulló-Lopez, *Europhys. Lett.* **14**, 557 (1991).

<sup>21</sup>L. Rebouta, M. F. da Silva, J. C. Soares, J. A. Sanz-García, E. Diéguez, and F. Agulló-Lopez, *Nucl. Instrum. Methods B* **64**, 189 (1992).

<sup>22</sup>C. Zaldo, C. Prieto, H. Dexpert, and P. Fessler, *J. Phys.* **3**, 4135 (1991).

<sup>23</sup>D. Kollwe, A. Kling, B. C. Grabmaier, T. Bremer, W. Heiland, and W. Zimmermann (unpublished).

<sup>24</sup>C. Zaldo, F. Agulló-Lopez, J. Garcia, A. Marielli, and S. Mobilio, *Solid State Commun.* **71**, 243 (1989).

<sup>25</sup>L. Kovács, L. Rebouta, J. C. Soares, M. F. da Silva, M. Hage-Ali, J. P. Stoquert, P. Siffert, C. Zaldo, Zs. Szaller, and K. Polgár, *Mater. Sci. Eng. B* **9**, 505 (1991).

<sup>26</sup>L. Kovács, L. Rebouta, J. C. Soares, M. F. da Silva, M. Hage-Ali, J. P. Stoquert, P. Siffert, J. A. Sanz-García, G. Corradi, Zs. Szaller, and K. Polgár, *J. Phys.* **5**, 781 (1993).

<sup>27</sup>P. Villars and L. D. Calvert, *Pearson's Handbook of Crystallographic Data for Intermetallic Phases* (American Society for Metals, Metals Park, OH, 1985).